WARWICK
THE UNIVERSITY OF WARWICK

Study of the slippage of particle / supercritical CO_2 two-phase flow

Lei Hou [a,b], Baojiang Sun [a]*, Xueyu Geng [c], Tingxue Jiang [b], Zhiyuan Wang [a]

[a] School of Petroleum Engineering, China University of Petroleum (East China), 66 Changjiang West Rd, Qingdao 266580, China

[b] SINOPEC Research Institute of Petroleum Engineering, Beijing 100101, China

[c] School of Engineering, The University of Warwick, Coventry, UK, CV4 7AL

Abstract In this paper, the slippage velocity and displacement between particles and supercritical CO_2 (SC-CO_2) were studied to reveal the particle-SC-CO_2 two-phase flow behavior. Visualization experiments were performed to directly measure the slippage velocity and displacement. Eight groups of experiments involving various pressures (7.89–10.96 MPa), temperatures (38.6–47.5 °C), particle diameters (0.3–0.85 mm), particle densities (2630 and 3120 kg/m^3) and SC-CO_2 flow rates (0.920–1.284 m/s) were conducted. The measured particle slippage velocities in the flowing direction were approximately 10.3 % of the SC-CO_2 flow rate. The measured particle slippage displacements were all at the centimeter level, which indicated that SC-CO_2 had a superior particle transporting capability that was similar to those of liquids even if it had a low viscosity that was similar to those of gases. A numerical model was built, and analytic slippage calculations were performed for SC-CO_2 for additional analyses. The density of SC-CO_2 was found to have a greater influence on the slippage than the viscosity. Moreover, a comparison of the slippage between SC-CO_2 and water showed that the particle slippage in water was constant, while the particle slippage in SC-CO_2 continually accumulated at an extremely slow rate.

Keywords: supercritical CO_2; two-phase flow; visualization experiments; analytic calculations; slippage behavior

* Corresponding author. Tel.: +86 532 86983137; fax: +86 532 86983137
E-mail address: sunbj1128@126.com (Baojiang Sun)

1. Introduction

Supercritical CO_2 (SC-CO_2), which has recently been introduced to petroleum engineering, can be used as a drilling or fracturing fluid and is an efficient and environmentally friendly petroleum engineering fluid. Basic research has been conducted on SC-CO_2 applications in drilling and fracturing processes in recent years [1–4]. Street et al. [5] and Khanpour et al. [6] treated drilling fluid waste using SC-CO_2 and obtained efficient results. Du et al. [7,8] developed a large-scale SC-CO_2 circulating platform and performed SC-CO_2 jet experiments. The results showed higher efficiency with the SC-CO_2 jet than with the water jet. Sun et al. [9] and Wu et al. [10] used experimental and numerical methods to study the adsorption-desorption properties of supercritical CO_2 in shale. Wang et al. [11,12] performed a friction coefficient calculation of SC-CO_2 pipe flow and improved the SC-CO_2 density calculation method.

All of the previous studies described above have mainly focused on single-phase SC-CO_2. However, solid phase (drilling cut or proppant) transport is one of the essential uses of fluids in petroleum engineering [13,14]. It is SC-CO_2 multi-phase flow rather than single-phase flow that occurs in most field applications. For instance, one of the primary tasks of SC-CO_2 as a fracturing fluid is carrying the proppant (fine ceramsite or sand) as deeply as possible into the fracture in the horizontal direction.

The low-viscosity and high-density features of SC-CO_2 shroud its transporting capability. Particles transported in gases, which have low viscosities compared to SC-CO_2, have more serious slippage than particles transported in liquids, which have high densities compared to SC-CO_2. It is unclear whether SC-CO_2 has a low transporting capability similar to gases, a superior capability similar to liquids, or a capability that is between those of gases and liquids. Hence, solid phase transport has become one of the technique bottlenecks when using SC-CO_2, and more studies on SC-CO_2 multi-phase flow are needed.

However, SC-CO_2 multi-phase flow research has rarely been conducted, even in supercritical fluids research where studies have mainly focused on chemical properties. Therefore, this paper examines SC-CO_2 and particle two-phase flow. Experiments were performed to directly measure the slippage velocity and displacement. The features of particle slippage in SC-CO_2 were analyzed by using a numerical model, and analytic calculations were derived. The results can be applied for the particle-SC-CO_2 two-phase flow analysis in particle tracing, fluidization, transportation, etc.

2. Materials and methods

2.1 Materials

Ceramic particles, which are widely used in the petroleum industry as proppant for fracturing, were chosen for their uniform density and sphericity. Two different densities (2630 kg/m^3 and 3120 kg/m^3) and meshes (0.3~0.85 mm in diameter) of particles were used. The ceramic particles were obtained from Down-hole Service Co. at the Shengli Oil Field (SINOPEC). CO_2 with a purity of 99.99 % was purchased from Tianyuan Gas Product Co. (Qingdao, China).

2.2 Apparatus and procedures

Experiments on particle motion following with supercritical CO_2 were conducted in a visualization apparatus. More detailed descriptions of the apparatus, the operating procedures and the data processes can be found in Hou et al. [15]. The experimental setup consists of an SC-CO_2 supply system and a visualization module. The CO_2 is heated by a water bath to the supercritical state. The transient flow rate is recorded by an electromagnetic flowmeter group [8]. The visualization module is composed of a visualization channel simulator and a high-speed camera system, as shown in Figure 1. The channel simulator consists of four identical units, which can be freely disassembled and combined. The simulated channel has a fixed width of 5 mm, a height of 50 mm and a length of 250 mm for each unit. Each unit has two pairs of observation windows, as shown in Figure 1, through which the particle movements are filmed. The maximum working pressure of the visualization module is 30 MPa. The high-speed camera is an OLYMPUS I-speed TR, which has a maximum resolution of 1280 × 1024 at a speed of 2000 fps. The light source (SHIBUYA JHP-40WP) is an LED cold-light illuminator, which does not affect the temperature of the SC-CO_2 in the stimulated channel.

During the experimental process, the high-speed camera system was placed on both sides of the second window from the SC-CO_2 inlet. A small amount of particles was mixed in from the inlet above the first window (from the SC-CO_2 inlet). The particle motion was recorded by the camera, and, simultaneously, the temperature, pressure and flow rate were all noted. Thus, each record of the particle motion has corresponding temperature, pressure and flow rate notes.

The experimental data were processed using the OLYMPUS I-speed control software. The diameter, horizontal velocity and displacement of the particle in each time unit were obtained using picture-by-picture analysis. The average uncertainty of the experimental apparatus and the method is 0.19 % [15].

2.3 Particle horizontal motion model

Numerical analyses were also applied to reveal the characteristics of the SC-CO_2 and particle two-phase flow. The particle motion model was built based on the Basset-Boussinesq-Oseen (BBO) equation [16]. Considering that the effects of flowing friction, wall effects and roughness on the particle-SC-CO_2 two-phase flow are still unclear, the particle horizontal motion model was built based on the following assumptions:

(1) The SC-CO_2 flow is a steady, uniform flow;

(2) The particle/particle and particle/wall interactions are ignored.

By analyzing the forces (drag force, virtual mass force and Basset force) acting on a single particle in the flowing SC-CO_2, the particle horizontal motion differential equation is

$$\frac{\pi d_p^3}{6}\rho_p\frac{d\upsilon_p}{dt}=\frac{\pi d_p^2}{8}\rho_f(\upsilon_f-\upsilon_p)^2 C_D-\frac{\pi d_p^3}{12}\rho_f\frac{d\upsilon_p}{dt}-\frac{3d_p^2}{2}(\pi\rho_f\mu)^{1/2}\int_0^t\frac{\frac{d\upsilon_p}{d\tau}}{\sqrt{t-\tau}}d\tau \tag{1}$$

where d_p is the diameter of the particle, ρ_p is the density of the particle, υ_p is the horizontal velocity of the particle, ρ_f is the SC-CO_2 density, υ_f is the SC-CO_2 flow rate, C_D is the drag coefficient, μ is the SC-CO_2 viscosity, t is the time, and τ is the relaxation time.

The drag coefficient (C_D) is the key parameter in the drag force expression. However, there are no relevant reports on the specific drag coefficient calculation in SC-CO_2. Hence, an auxiliary equation set is established based on the power-law settling velocity calculation [15] to solve the drag coefficient indirectly. The equation set is

$$\begin{cases} C_D=\dfrac{4g(\rho_p-\rho_f)d_p}{3\upsilon_\infty^2\rho_f} \\ \upsilon_\infty=\dfrac{\mu}{\rho_f d_p}[0.1196(\dfrac{\rho_p}{\rho_f})^2-0.1216\dfrac{\rho_p}{\rho_f}-0.2961]Ar^{[-0.214\ln(\frac{\rho_p}{\rho_f})+0.8241]} \\ Ar=\dfrac{g(\rho_p-\rho_f)\rho_f d_p{}^3}{\mu^2} \end{cases} \tag{2}$$

where υ_∞ is the terminal settling velocity of particles in SC-CO_2, g is the acceleration due to gravity, and Ar is the particle Archimedes number.

The Basset force, which is also called the history force, is caused by the relative acceleration between the particles and the SC-CO_2. The Basset force expression in Eq. (1) is an integration and could be solved using the methods of Shenhua et al. [17] and Bombardelli et al. [18], who proved the convergence of the Basset force expression. The fractional integral method can be used to eliminate the integral singularity. The trapezoid formula can then be applied to discretize the integral term. The approximation of the integral term is given by

$$\int_0^t \frac{\frac{d\upsilon_p}{d\tau}}{\sqrt{t-\tau}}d\tau \approx \frac{h}{2}\left(\frac{a_0}{\sqrt{i\cdot h}} + 2\sum_{j=2}^{i-2}\frac{a_j}{\sqrt{i\cdot h - j\cdot h}} + \frac{a_{i-1}}{\sqrt{h}}\right) + (a_i + a_{i-1})\sqrt{h} \qquad (3)$$

where h is the time unit, a_0 is the initial (t=0) particle acceleration, and a_i is the particle horizontal acceleration at moment t_i.

Combining Eqs. (1), (2) and (3), the governing equation for the particle horizontal motion model can be given. In this model, the drag coefficient (C_D) is calculated by a new indirect method. The new method is based on the SC-CO_2 experiment [15] and is therefore more suitable for the SC-CO_2 case than other methods based on conventional fluid experiments.

The particle horizontal motion model is discretized using the Euler method and solved by programming in VB.NET.

3 Results and discussion

3.1 Experimental results

Eight groups of experiments were conducted under various temperature, pressure and particle conditions, as shown in Table 1. In each group of experiments, at least ten particles were selected randomly and processed to obtain a set of horizontal velocities and displacements. For a single particle, the motion can be affected by particle shape, roughness, wall effects, etc., which may induce strong randomness in its velocity and displacement. Therefore, the average values of the particle velocity and displacement are presented in Table 1.

The average particle velocities in the flow direction fall in the range of 0.843–1.204 m/s, which reach an average of 89.7 % of the $SC\text{-}CO_2$ flow velocity. The average slippage displacements fall in the range of 0.0135–0.0341 m and are all at the centimeter level. The directly measured slippage velocities and displacements between the particles and the $SC\text{-}CO_2$ were relatively small. Based on experimental measurements, $SC\text{-}CO_2$ was found to have a superior particle transporting capability that was similar to a liquid even if it had a low viscosity that was similar to that of a gas.

3.2 Verification of the particle horizontal motion model

The experimental results are used to verify the particle motion model. During the experiments, the frame rate of the camera was set to 1/4000 s. The directly measured parameters were the particle horizontal velocity and displacement in each time unit, which was 1/4000 s. The particle inlet (as shown in Fig. 1) was selected as the origin. Based on the relative position between the particle inlet and the observation windows, the center coordinate of the second window is known. According to the coordinates of the window center, the particle horizontal displacement (L_1) from the inlet can be measured at the time when it enters the observation window. Similarly, the displacement (L_2) can be obtained at the moment when the particle moves out of the window. During this displacement, the particle horizontal velocity and displacement in each time unit can be measured by image analysis. The numerical velocity and displacement in the same period are then calculated and compared with the experimental results, verifying the particle motion model.

In each time unit, the particle acceleration is assumed to be uniform. The particle displacement in each unit is calculated by the average velocity. According to the experimental conditions, the initial conditions are

$$\begin{cases} \upsilon_{p(0)} = 0 \\ \dfrac{d\upsilon_p}{dt}_{(0)} = \dfrac{3\rho_f}{4d_p\rho_p}(\upsilon_f)^2 C_D \\ L_{(0)} = 0 \end{cases} \quad (4)$$

The boundary conditions are

$$\begin{cases} L_{(n1)} = L_1 \\ L_{(n2)} = L_2 \end{cases} \quad (5)$$

A specific particle is taken as an example to illustrate the verification process. This particle has a diameter of 0.647 mm and a density of 3120 kg/m^3. The experimental temperature and pressure are 45.9 °C and 10.96 MPa, respectively. The SC-CO_2 flow rate is 1.085 m/s. The measured horizontal displacement L_1 is 0.114 m, and L_2 is 0.146 m. Based on the given conditions and Eqs. (1), (2), (3), (4) and (5), the numerical velocity and displacement are calculated and compared with the measured values. The results are shown in Figure 2. The straight line in Figure 2 (a) represents the velocity predicted by the particle motion model. The scattered points are the experimentally measured velocities. The higher and lower points in Figure 2 (b) are the numerical and experimental displacements of the particle, respectively. The SC-CO_2 displacement is used as a reference. The slippage between the SC-CO_2 and the particle is approximately 0.025 m. The calculated velocities and displacements have average errors of 4.90 % and 1.32 %, respectively, which match the experimental results well.

More comparisons were conducted to test the accuracy of the slippage equation, as shown in Table 2. Five particles from each group of experiments in Table 1 were randomly selected, processed using the same method as described above and compared with the calculated results under the same conditions. The average errors of the particle motion model are summarized in Table 2. The errors are all positive values, indicating that the calculated results exceed the measurements. Preliminary analysis suggests that the wall effects hinder the particle motion and slightly reduce the measured particle velocities. Overall, the average velocity errors of the eight experimental groups ranged from 3.48 % to 8.23 %. The average displacement errors were between 1.25 % and 5.49 %. Therefore, the particle motion model provides accurate predictions and can be used to evaluate particle transport in SC-CO_2.

3.3 Derivation of the slippage velocity and displacement analytic calculations

3.3.1 Neglecting the Basset force

To derive the analytic formulas, the effects of the Basset force on the slippage velocity and displacement were analyzed. According to the measured fracture pressure gradient and the geothermal gradient in the field [19,20], SC-CO_2 conditions of 50 MPa and 120 °C were chosen as an example; these conditions are close to the underground conditions at a depth of 2000–3000 m during the fracturing operation. The density and viscosity of SC-CO_2 under these conditions were taken from the National Institute of Standards and Technology website [21] and are 763.68 kg/m^3 and 0.068 mPa·s, respectively. The SC-CO_2 flow rate is assumed to be 1 m/s based on the common field pump rates and fracture sizes [22]. The chosen particle density is 3120 kg/m^3, and the average diameter is 0.6 mm. The calculated particle velocity and displacement, with and without the Basset force, are shown in Figure 3.

The particle velocity differences based on the Basset force fall in the range of 2.2–6.2 %, and the average value is 5.4 %, as shown in Figure 3 (a). The particle displacement differences by Basset force in Figure 3 (b) are within the range of 0.97–5.5 %, and the average value is 4.5 %. These differences are small and can be ignored in the particle transport research. Therefore, the effects of the Basset force on the slippage velocity and displacement can be ignored.

3.3.2 Derivation of the horizontal velocity and slippage analytic formulas

When the Basset force is ignored, Eq. (1) becomes

$$\frac{\pi d_p^3}{6}\rho_p\frac{d\upsilon_p}{dt}=\frac{\pi d_p^2}{8}\rho_f(\upsilon_f-\upsilon_p)^2C_D-\frac{\pi d_p^3}{12}\rho_f\frac{d\upsilon_p}{dt} \tag{6}$$

Eq. (6) can also be written as

$$\frac{d\upsilon_p}{dt}=\frac{3\rho_f C_D}{2d_p(2\rho_p+\rho_f)}(\upsilon_f-\upsilon_p)^2 \tag{7}$$

Letting

$$T_r=\frac{2d_p(2\rho_p+\rho_f)}{3\rho_f C_D} \tag{8}$$

Then, Eq. (7) can then be simplified to

$$(\upsilon_f-\upsilon_p)^{-2}d\upsilon_p=\frac{1}{T_r}dt \tag{9}$$

The drag coefficient (C_D) is solved by Eq. (2) and is a constant value under certain pressure and temperature conditions according to the previous study on particle settling in SC-CO_2 [15]. Therefore, Eq. (9) can be integrated directly. The initial particle horizontal velocity is assumed to be zero. The slippage velocity (S_V) is calculated as

$$S_V=\upsilon_f-\upsilon_p=\frac{T_r\cdot\upsilon_f}{t\cdot\upsilon_f+T_r} \tag{10}$$

The slippage displacement (S_D), defined as the relative displacement between the particle and the SC-CO_2 in the horizontal direction, can be derived based on Eq. (10)

$$S_D = \upsilon_f \cdot t - \int_0^t \upsilon_p dt \tag{11}$$

By combining Eqs. (10) and (11), the slippage displacement equation is given by

$$S_D = T_r \cdot ln(\frac{\upsilon_f \cdot t + T_r}{T_r}) \tag{12}$$

Eqs. (10) and (12) are the first analytic solutions for particle slippage velocity and displacement in SC-CO_2, which can be applied for the particle-SC-CO_2 two-phase flow analysis in particle tracing, fluidization, transportation, etc.

3.4 Numerical analysis of particle relative motion in SC-CO_2

The particle-SC-CO_2 slippage was analyzed using the slippage velocity and displacement calculations. The most widely used ceramsite was chosen as the particle type and has a density of 3120 kg/m^3. The particle diameter was 0.6 mm, which is the average value of the commonly used proppant.

3.4.1 Flow rate effects on the particle-SC-CO_2 slippage

The slippage velocity and displacement under various SC-CO_2 flow rate conditions are shown in Figure 4. The pressure and temperature conditions of the SC-CO_2 were 50 MPa and 120 °C, which are close to the underground conditions at a depth between 2000 m and 3000 m during the fracturing operation. The practical flow rate in actual underground fractures is determined by the pump rate, fracture size, leak off, etc. Hence, the flow rates used in the evaluation were in the range from 0.5–2.5 m/s [22].

The slippage velocity decreases rapidly with increasing particle velocity. After 0.15 s, the slippage velocity decreases extremely slowly. Different flow rates have little effect on the slippage velocity, as shown in Figure 4 (a).

The slippage displacement is the accumulated relative displacement between the particle and the $SC\text{-}CO_2$. In the early stage (before 10 s), slippage displacement increases rapidly, as shown in Figure 4 (b). The increasing rate then drops with decreasing slippage velocity, and the curve becomes a straight line with a small slope. All of the slippage displacements are at the centimeter level and far below the underground fracture length in formation, which is typically at the ten-meter or even hundred-meter level [23]. Thus, the relative displacement between the proppant and $SC\text{-}CO_2$ is negligible in field applications, where the proppant is transported deep into the fracture along the length direction. $SC\text{-}CO_2$ is proven to be qualified for proppant transport in the horizontal direction under various flow rate conditions.

3.4.2 Effects of $SC\text{-}CO_2$ density and viscosity on slippage

Similar to the effect of the flow rate on the slippage velocity, the effects of the $SC\text{-}CO_2$ density and viscosity on the slippage velocity are inconspicuous. Therefore, only the slippage displacement was analyzed, as shown in Figure 5. The slippage displacements decrease with increasing $SC\text{-}CO_2$ density and viscosity. Even under relatively low density (300 kg/m^3) and viscosity (0.01 mPa·s) conditions, the slippage displacements are all at the centimeter level and less than 0.08 m, which demonstrates the particle transport ability of $SC\text{-}CO_2$.

Two interesting differences were discovered between Figure 5 (a) and Figure 5 (b). One difference is that a viscosity increase of a factor of ten thousand reduces the slippage from 0.08 m to 0.04 m, while a density increase of a factor of less than four reduces the slippage by the same amount. The other difference is that the reduction rate of the slippage decreases with increasing viscosity, while the reduction rate increases with increasing density. In Figure 5 (a), the slippage reduces slightly when the $SC\text{-}CO_2$ density increases from 300 kg/m^3 to 500 kg/m^3.

However, the slippage decreases by 50 % (from approximately 0.06 m to 0.03 m) when the density increases from 900 kg/m^3 to 1100 kg/m^3. In Figure 5 (b), the effect of the SC-CO_2 viscosity follows a reverse rule in which the reduction rate of the slippage decreases with increasing viscosity.

Past research views the viscosity as the main physical criterion of fracturing fluids for proppant transport because a high viscosity prevents the proppant from settling in the vertical direction. However, the above analysis reveals that the density of SC-CO_2 exerts a greater influence on particle slippage than the viscosity. The density of SC-CO_2, rather than only the viscosity, should be evaluated for effective proppant transport.

3.4.3 Comparison of the slippage in SC-CO_2 and water

The slippage velocity and displacement in SC-CO_2 and water were compared. The density and viscosity of water are 1000 kg/m^3 and 1 mPa·s, respectively. The particle diameter and density are 0.6 mm and 3120 kg/m^3, respectively. The pressure and temperature of SC-CO_2 are 50 MPa and 120 °C, respectively. The fluid flow rates are both 1 m/s.

For water, Eq. (2) is unsuitable for the drag coefficient solution. Instead, the Stokes drag coefficient equation (C_D=24 / Re) is applied [24]. The slippage equations for water are given by

$$\begin{cases} S_{Vw} = e^{-\frac{t}{T_{rw}}} \upsilon_{fw} \\ S_{Dw} = \upsilon_{fw} T_{rw} (1 - e^{-\frac{t}{T_{rw}}}) \end{cases} \tag{13}$$

where

$$T_{rw} = \frac{d_p^2 (2\rho_p + \rho_{fw})}{36 \mu_w} \tag{14}$$

The comparison results, which were calculated using Eqs. (8), (10), (12), (13) and (14), are shown in Figure 6. Both of the slippage velocities in SC-SO_2 and water exhibited nearly the same rate of decrease. The main difference was that the slippage velocity rapidly decreased to zero in water, whereas it decreased at an extremely slow rate after a sharp decrease and did not decrease to zero in SC-CO_2 (Fig. 6 (a)). This difference indicates that particles flowing with water can reach the water flow velocity, although they cannot reach the flow velocity when flowing with SC-CO_2.

The slippage displacement reflects the corresponding slippage velocity law, as shown in Figure 6 (b). The slippage displacement in the water increased rapidly to a constant value because the slippage velocity in water can decrease to zero. However, the slippage displacement curve in SC-CO_2 approached a straight line with a small slope because the slippage velocity always exists and the slippage displacement continually increases, even after 100 s.

Although the experiments conducted here demonstrated the superior particle transporting capability of SC-CO_2 and showed that it is similar to a liquid, the additional numerical analysis revealed the detailed differences in the slippage velocity and displacement between SC-CO_2 and water. However, it is worth noting that the differences in the slippage velocities (less than 10 % of the flowing velocity) and displacements (centimeter level) are relatively insignificant and negligible under the conditions of petroleum engineering applications. In addition, the vertical particle motion also indicated that the particle settling velocity in SC-CO_2 was similar to that for liquid CO_2 [15]. By synthesizing the horizontal and vertical particle motion characteristics in SC-CO_2, the conclusion that SC-CO_2 has superior particle transporting capability is emphasized.

4 Conclusions

In this work, experimental and numerical methods were applied to study the slippage in particle-SC-CO_2 two-phase flow. The experimentally measured slippage velocity (10.3 % of the SC-CO_2 flowing rate) and displacement (centimeter level) indicated that SC-CO_2 has a superior particle transporting capability that is similar to those of liquids. The analytic calculations for the slippage velocity and displacement of SC-CO_2 were derived and applied for additional numerical analyses. The density of SC-CO_2 was found to have a greater influence on particle slippage than the viscosity. Hence, the density of SC-CO_2, rather than only the viscosity, should be evaluated for effective particle transport. A comparison of the slippage between SC-CO_2 and water revealed that both of the slippage evolution had approximately the same behavior. However, the slippage velocity in water approached zero, while it continually decreased at an extremely slow rate after the same sharp decrease in SC-CO_2. Thus, the slippage displacement in water tended to be constant, while it continually increased at an extremely slow rate in SC-CO_2. These differences in the slippage velocity (less than 10 % of the flowing velocity) and displacement (centimeter level) are relatively insignificant and negligible under the conditions of engineering applications.

Acknowledgements

This work was supported by the Natural Science Foundation of China (U1262202, 5121006)

Appendix

d_p [m] diameter of the particle

ρ_p [kg/m^3] density of the particle

υ_p [m/s] horizontal velocity of the particle

ρ_f [kg/m^3] SC-CO_2 density

ρ_{fw} [kg/m^3] water density

υ_f	[m/s]	SC-CO_2 flow rate
υ_{fw}	[m/s]	water flow rate
μ	[Pa·s]	SC-CO_2 viscosity
μ_w	[Pa·s]	water viscosity
t, τ	[s]	time
C_D	[–]	drag coefficient
υ_∞	[m/s]	terminal settling velocity of particle in SC-CO_2
g	[m/s^2]	gravity
Ar	[–]	particle Archimedes number, $Ar = \frac{g(\rho_p - \rho_f)\rho_f d_p^{\,3}}{\mu^2}$
h	[s]	time unit
a_i, a_j	[m/s^2]	particle horizontal acceleration at different moments
$\upsilon_{p(i)}$	[m/s]	particle horizontal velocity at moment t_i
L_1, L_2, $L_{(i)}$	[m]	particle horizontal displacement at different moments
T_r, T_{rw}	[–]	procedure parameter of formula derivation
S_V	[m/s]	slippage velocity between the particle and SC-CO_2
S_D	[m]	slippage displacement between the particle and SC-CO_2
S_{Vw}	[m/s]	slippage velocity between the particle and water
S_{Dw}	[m]	slippage displacement between the particle and water
e	[–]	Napierian logarithm
T	[ºC]	temperature of SC-CO_2
P	[MPa]	pressure of SC-CO_2

References

[1] L. Zhang, S. Ren, B. Ren, W. Zhang, Q. Guo, L. Zhang, Assessment of CO_2 storage capacity in oil reservoirs associated with large lateral/underlying aquifers: case studies from China, Int. J. Greenhouse Gas Contr. 5 (2011) 1016-1021.

[2] B. Ren, L. Zhang, H. Huang, S. Ren, G. Chen, H. Zhang, Performance evaluation and mechanisms study of near-miscible CO_2 flooding in a tight oil reservoir of Jilin oilfield China, J. Nat. Gas Sci. Eng. 27 (2015) 1796-1805.

[3] R.A. Chadwick, D.J. Noy, S. Holloway, Flow processes and pressure evolution in aquifers during the injection of supercritical CO_2 as a greenhouse gas mitigation measure, Petrol. Geosci. 15 (2009) 59–73.

[4] G. Zhang, C. Taberner, L. Cartwright, T. Xu, Injection of supercritical CO_2 into deep saline carbonate formations: predictions from geochemical modeling, SPE J. 16 (2011) 959–967.

[5] C.G. Street, C. Tesche, S. Guigard, Treatment of hydrocarbon-based drilling waste using supercritical carbon dioxide, SPE Drill. Completion 9 (2009) 413–417.

[6] R. Khanpour, M.R. Sheikhi-Kouhsar, F. Esmaeilzadeh, D. Mowla, Removal of contaminants from polluted drilling mud using supercritical carbon dioxide extraction, J. Supercrit. Fluids 88 (2014) 1–7.

[7] Y.K. Du, R.H. Wang, H.J. Ni, H.J. Huo, Z.Y. Huang, W.M. Yue, H.X. Zhao, B. Zhao, Rock-breaking experiment with supercritical carbon dioxide jet, J. Chin. Univ. Petrol. 36 (2012) 93–96.

[8] Y. Du, R. Wang, H. Ni, M. Li, W. Song, H. Song, Determination of rock-breaking performance of high-pressure supercritical carbon dioxide jet, J. Hydrodynamics B 24 (2012) 554–560.

[9] B. Sun, Y. Zhang, Q. Du, Z. Shen, Property evaluation of CO_2 adsorption and desorption on shale, J. Chin. Univ. Petrol. 37 (2013) 95-99.

[10] T. Wu, Q. Xue, X. Li, Y. Tao, Y. Jin, C. Ling, S. Lu, Extraction of kerogen from oil shale with supercritical carbon dioxide: molecular dynamics simulations, J. Supercrit. Fluids 107 (2016) 499–506.

[11] Z. Wang, B. Sun, J. Wang, L. Hou, Experimental study on the friction coefficient of supercritical carbon dioxide in pipes, Int. J. Greenhouse Gas Contr. 25 (2014) 151–161.

[12] Z. Wang, B. Sun, L. Yan, Improved density correlation for supercritical CO_2, Chem. Eng. Technol. 38 (2015) 75–84.

[13] N.A. Patankar, D.D. Joseph, J. Wang, R.D. Barree, M. Conway, M. Asadi, Power law correlations for sediment transport in pressure driven channel flows, Int. J. Multiphase Flow 28 (2002) 1269–1292.

[14] M.A. Biot, W.L. Medlin, Theory of Sand Transport in Thin Fluids, SPE, 1985, p. 14468.

[15] L. Hou, B. Sun, Z. Wang, Q. Li, Experimental study of particle settling in supercritical carbon dioxide, J. Supercrit. Fluids 100 (2015) 121–128.

[16] E.E. Michaelides, Review: transient equation of motion for particles, bubbles, and droplets, J. Fluids Eng. 119 (1997) 233–247.

[17] H. Shehua, L. Wei, C. Liangjun, On numerical method of resolving discrete solid particles motion equation and its applications, J. Hydrodynamics 14 (1999) 51–61.

[18] F.A. Bombardelli, A.E. González, Y.I. Niño, Computation of the particle basset force with a fractional-derivative approach, J. Hydraul. Eng. 134 (2008) 1513–1519.

[19] N.C. Dutta, Geopressure prediction using seismic data: Current status and the road ahead,

Geophysics 67 (2002) 2012–2041.

[20] S. Cao, I. Lerche, Geohistory, thermal history and hydrocarbon generation history of Navarin Basin COST No.1 well Bering Sea Alaska, J. Petrol. Geol. 12 (1989) 325–352.

[21] National Institute of Standards and Technology, NIST, Chemistry WebBook, 2014. http://webbook.nist.gov/chemistry/fluid/.

[22] J. Micheal, Economides, in: Reservoir Stimulation, Petroleum Industry Press, Beijing, 3rd ed., (2002), pp. 145–151.

[23] X.E. Refunjol, K.M. Keranen, J.H. Le Calvez, K.J. Marfurt, Integration of hydraulically induced microseismic event locations with active seismic attributes: A North Texas Barnett Shale case study, Geophysics 77 (2012) KS1–KS12.

[24] E. Novotny, Proppant transport, in: Proceedings of the 52nd Annual Fall Technical Conference and Exhibition of the Society of Petroleum Engineers, Vol. 2, Denver, 9-12 October, 1977.

Figure List

Fig. 4 Particle slippage velocity and displacement in SC-CO_2 under various flow rate conditions. The particle density and diameter are 3120 kg/m^3 and 0.6 mm, respectively. The temperature and pressure of SC-CO_2 are 120 °C and 50 MPa, respectively. (a) Particle slippage velocity in SC-CO_2 under various flow rate conditions. The flow rates from top to bottom are 2.5 m/s ■, 2.0 m/s ●, 1.5 m/s ▲, 1.0 m/s ▼ and 0.5 m/s . (b) Particle slippage displacement in SC-CO_2 under various flow rate conditions. The flow rates from top to bottom are 2.5 m/s ■, 2.0 m/s ●, 1.5 m/s ▲, 1.0 m/s ▼ and 0.5 m/s .

Fig. 5 Particle slippage displacement under various SC-CO_2 density and viscosity conditions. The particle density and diameter are 3120 kg/m^3 and 0.6 mm, respectively. (a) Particle slippage displacement under various SC-CO_2 density conditions. The viscosity and flow rate of SC-CO_2 are 0.068 mPa·s and 1 m/s, respectively. The SC-CO_2 densities from top to bottom are 300 kg/m^3 ■, 500 kg/m^3 ●, 700 kg/m^3 ▲, 900 kg/m^3 ▼ and 1100 kg/m^3 . (b) Particle slippage displacement under various SC-CO_2 viscosity conditions. The density and flow rate of SC-CO_2 are 763.68 kg/m^3 and 1 m/s, respectively. The SC-CO_2 viscosities from top to bottom are 0.01 mPa·s ■, 0.1 mPa·s ●, 1.0 mPa·s ▲, 10.0 mPa·s ▼ and 100.0 mPa·s .

Fig. 6 Comparison of the particle slippage velocity and displacement in SC-CO_2 and water. The particle density and diameter are 3120 kg/m^3 and 0.6 mm, respectively. The temperature and pressure of SC-CO_2 are 120 °C and 50 MPa, respectively. The density and viscosity of water are 1000 kg/m^3 and 1 mPa·s, respectively. The flow rates are both 1 m/s. (a) Comparison of the particle slippage velocity in SC-CO_2 and water. The ■ points represent the slippage velocities in SC-CO_2, and the ● points represent the slippage velocities in water. (b) Comparison of the particle slippage displacement in SC-CO_2 and water. The upper points ■ represent the slippage displacements in SC-CO_2, and the lower points ● represent the slippage displacements in water.

Figure 1

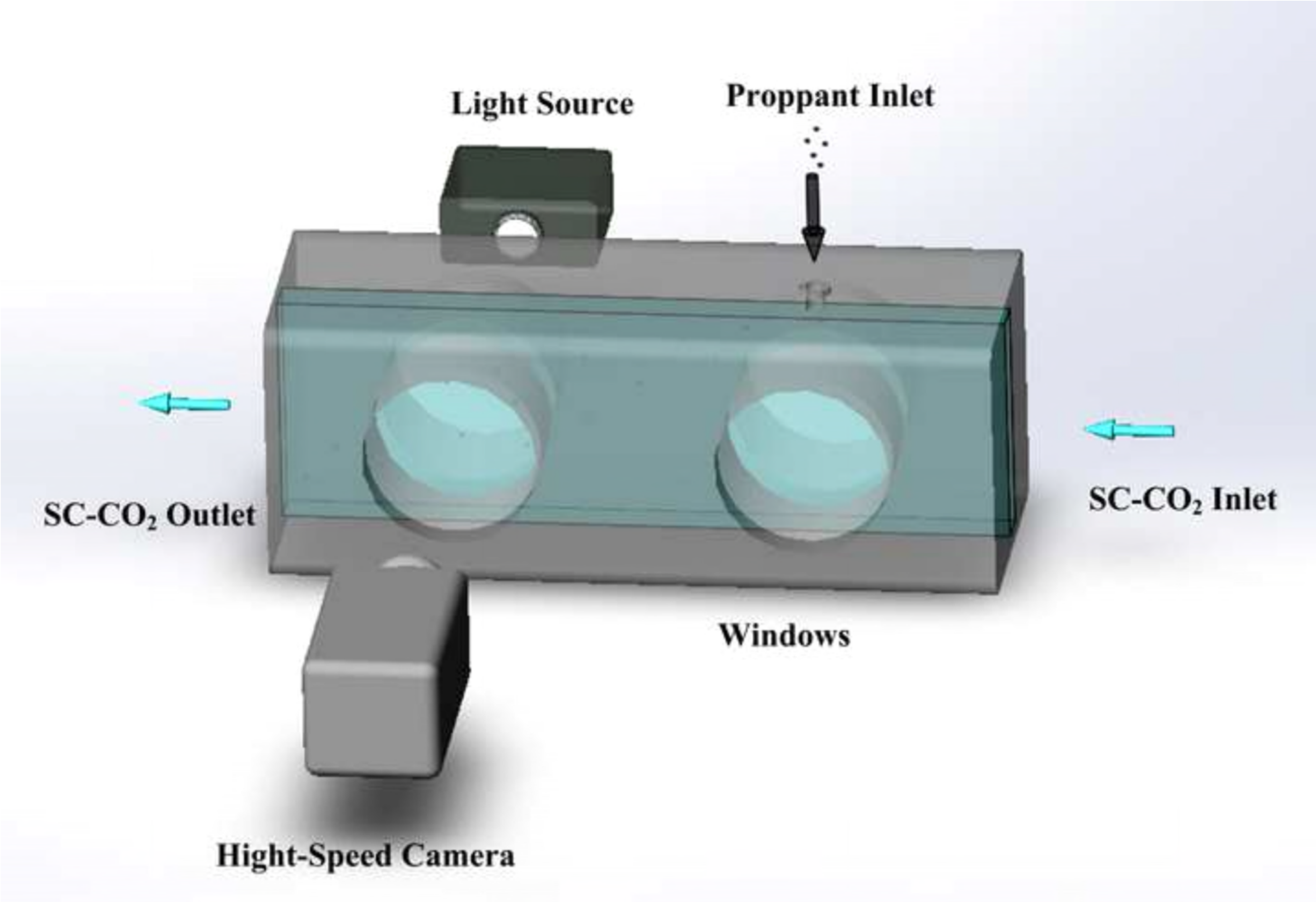
Light Source
Proppant Inlet
SC-CO_2 Outlet
SC-CO_2 Inlet
Windows
Hight-Speed Camera

Figure 2 (a)

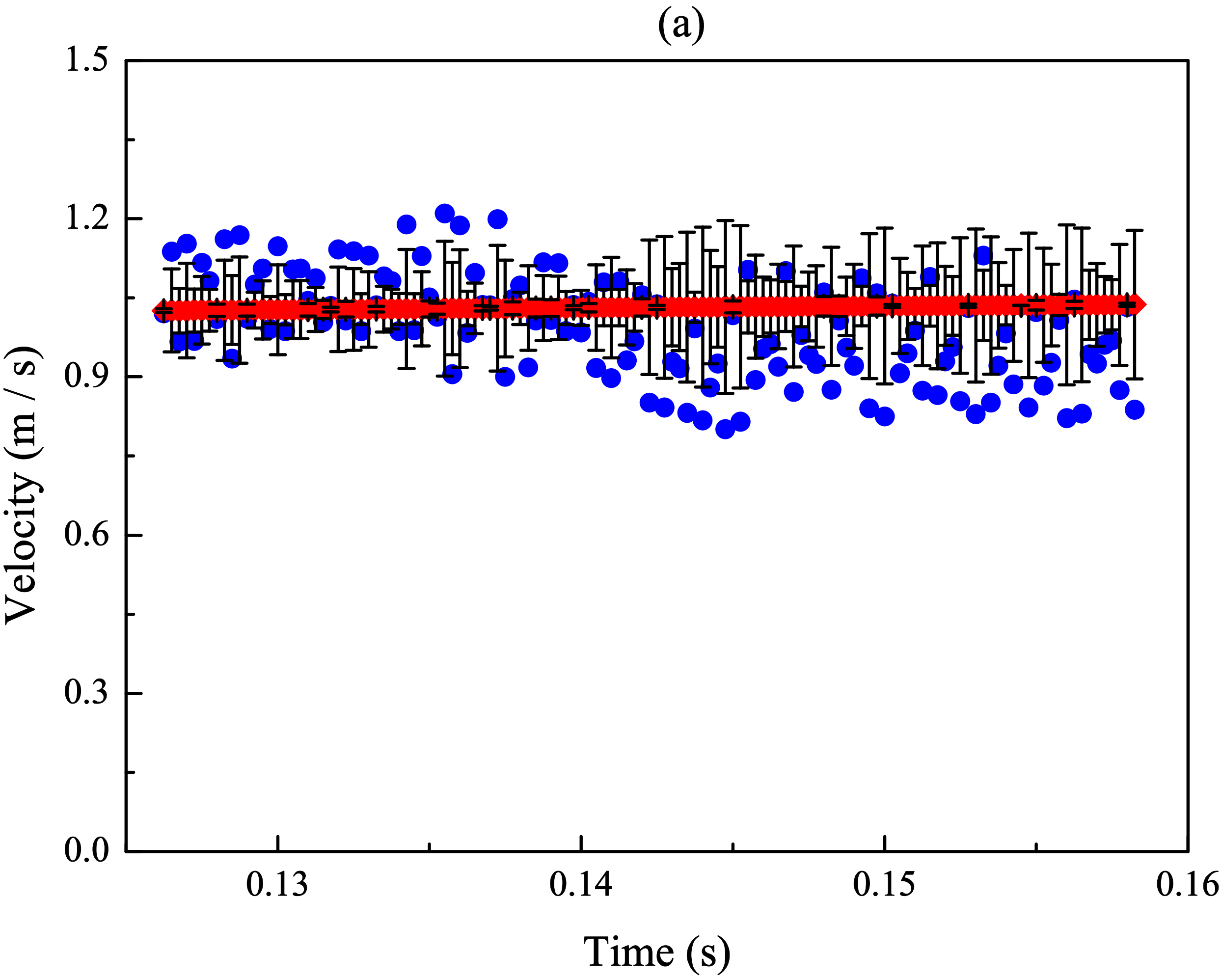

Figure 2 (b)

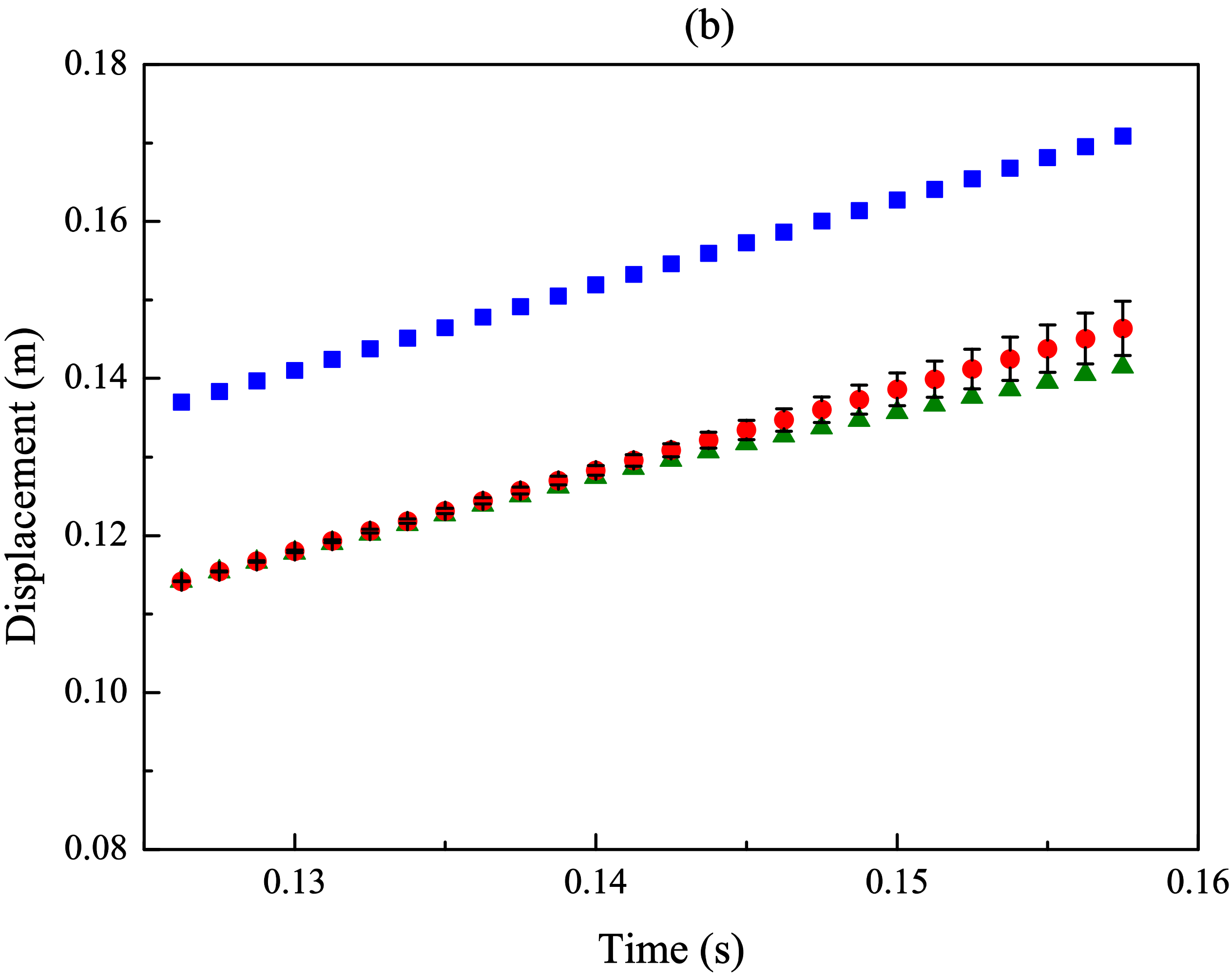

Figure 3 (a)

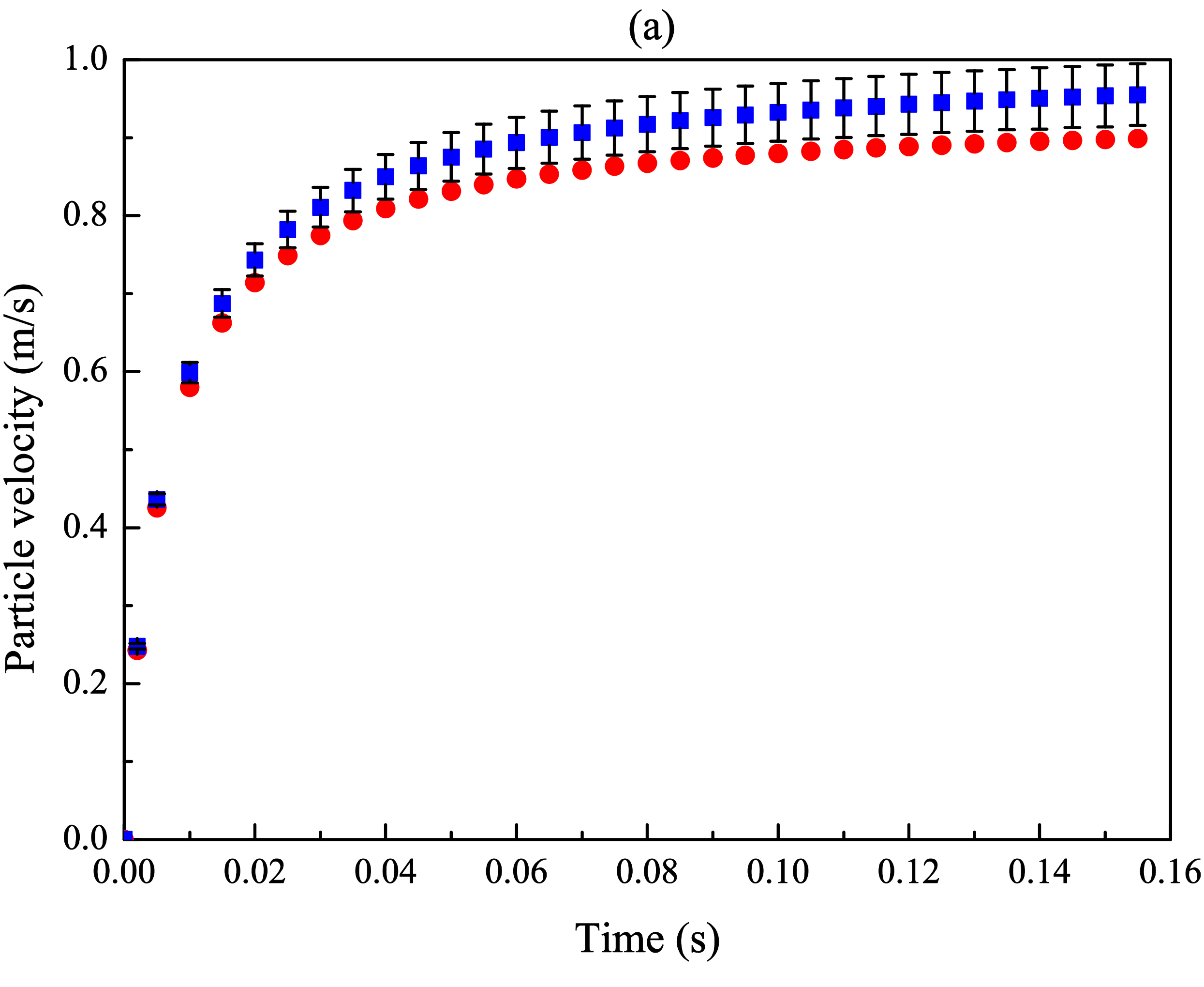

(a)
1.0
0.8
0.6
0.4
0.2
0.0
Particle velocity (m/s)
0.00
0.02
0.04
0.06
0.08
0.10
0.12
0.14
0.16
Time (s)

Figure 3 (b)

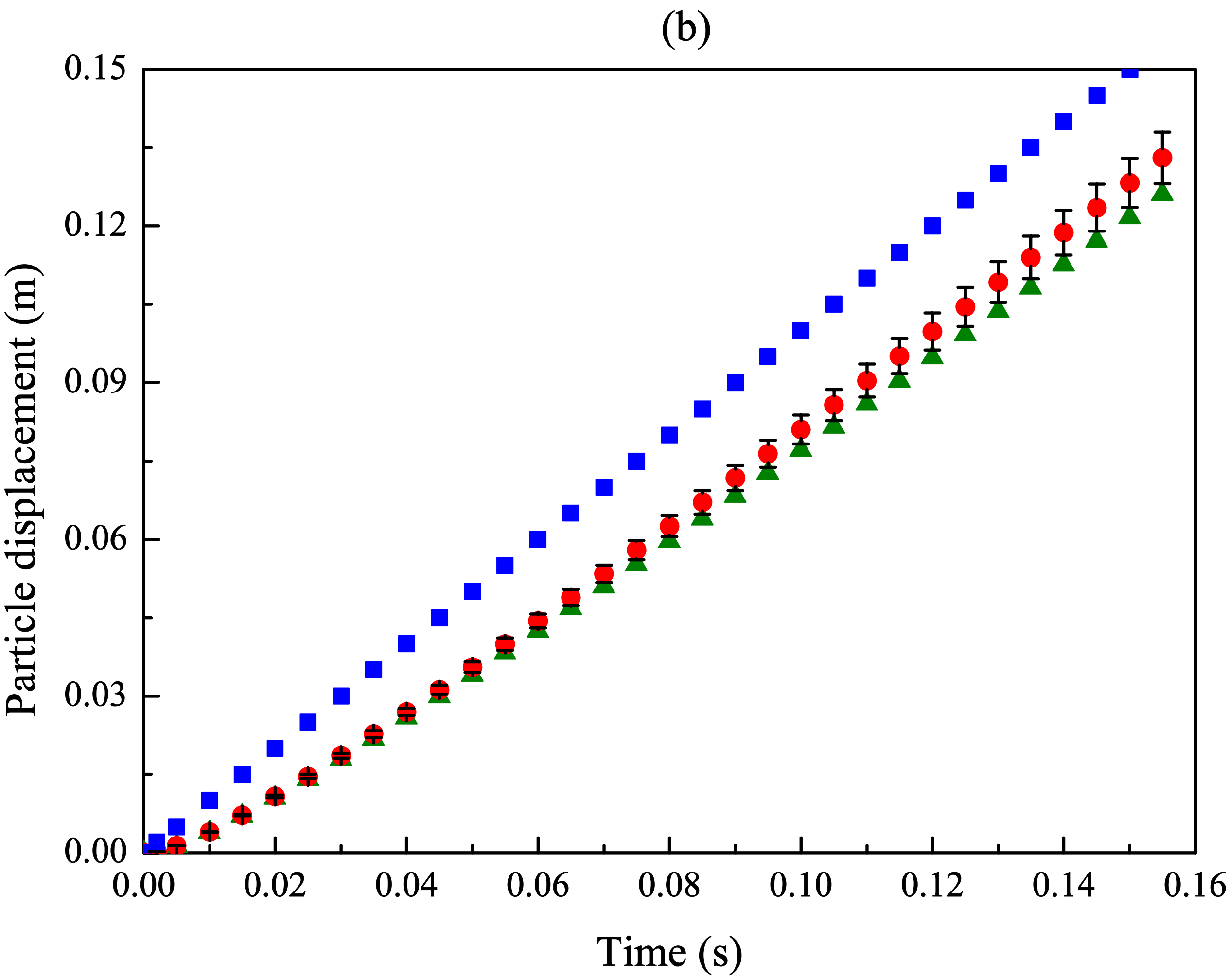

(b)
0.15
0.12
0.09
0.06
0.03
0.00
Particle displacement (m)
0.00
0.02
0.04
0.06
0.08
0.10
0.12
0.14
0.16
Time (s)

Figure 4 (a)

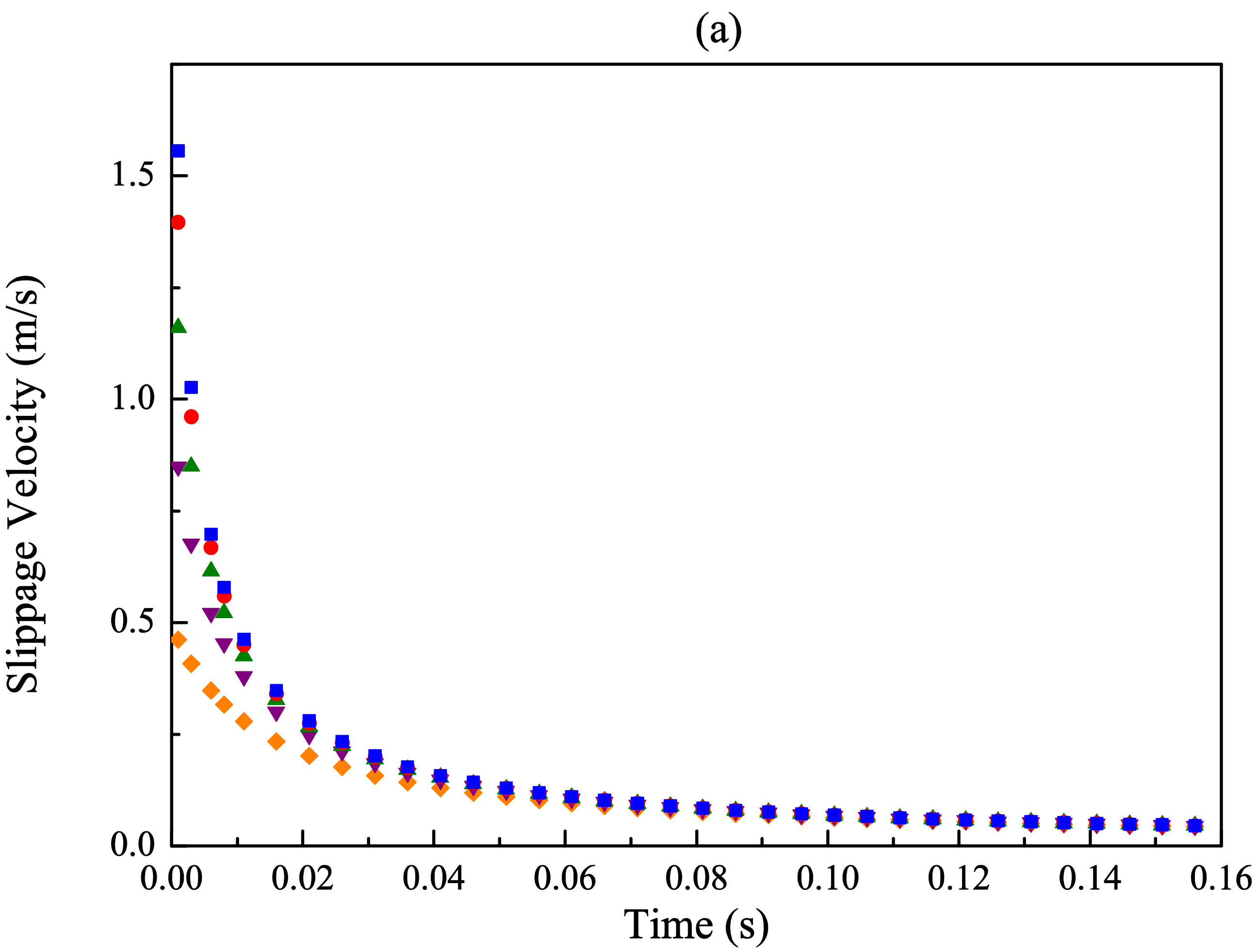
(a)
Slippage Velocity (m/s)
0.0
0.5
1.0
1.5
0.00
0.02
0.04
0.06
0.08
0.10
0.12
0.14
0.16
Time (s)

Figure 4 (b)

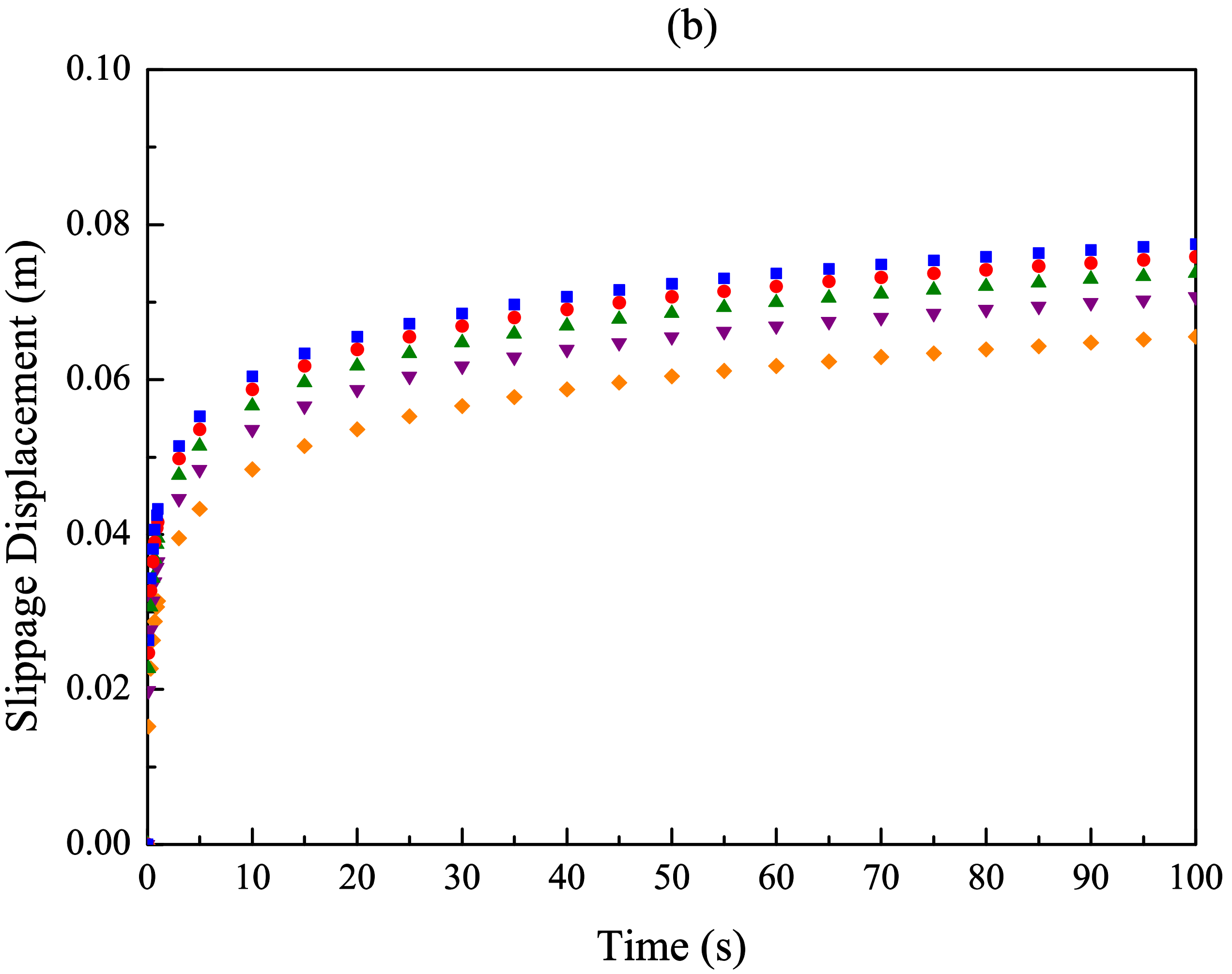

(b)
0.10
0.08
0.06
0.04
0.02
0.00
Slippage Displacement (m)
0
10
20
30
40
50
60
70
80
90
100
Time (s)

Figure 5 (a)

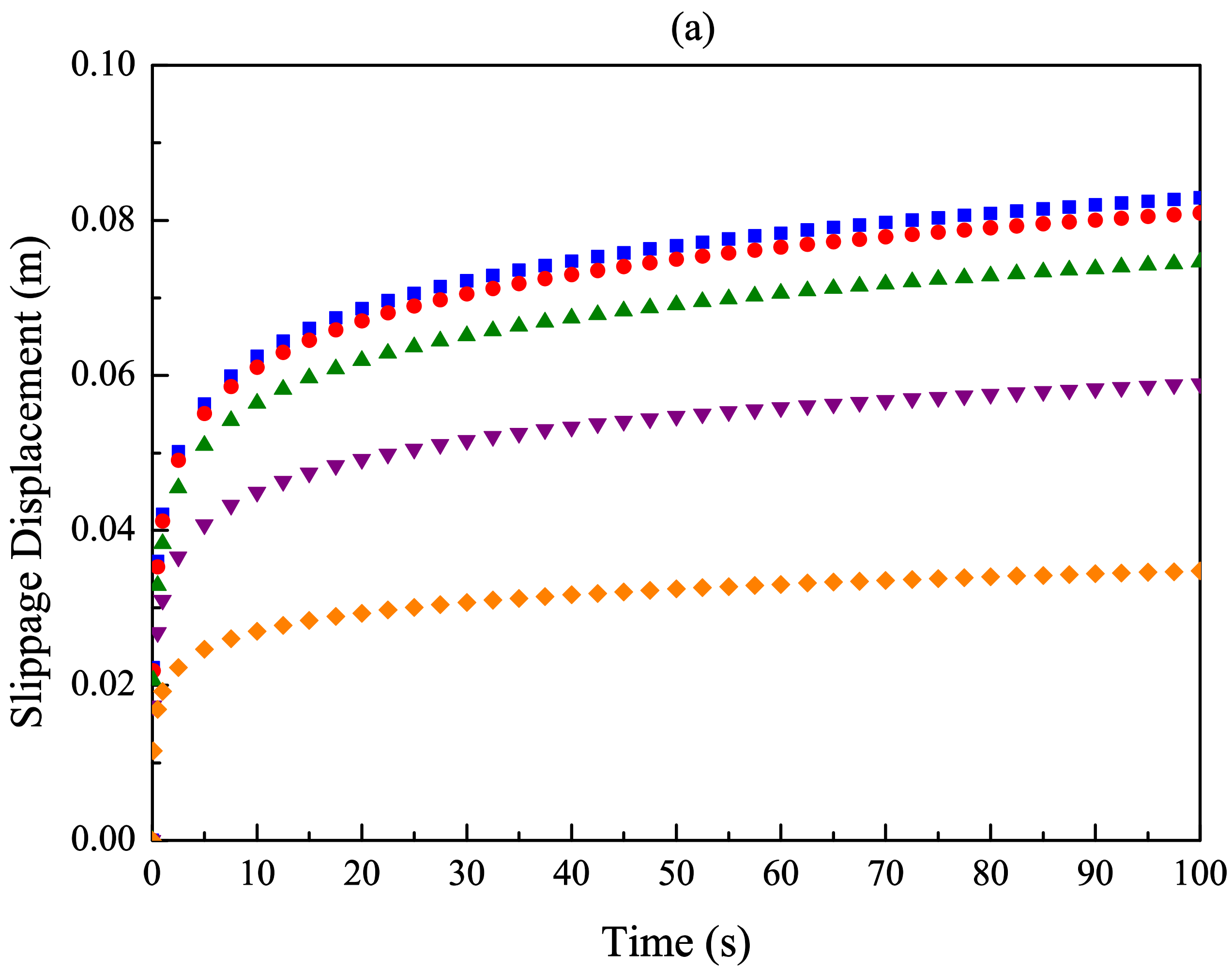
(a)
Slippage Displacement (m)
0.00
0.02
0.04
0.06
0.08
0.10
0
10
20
30
40
50
60
70
80
90
100
Time (s)

Figure 5 (b)

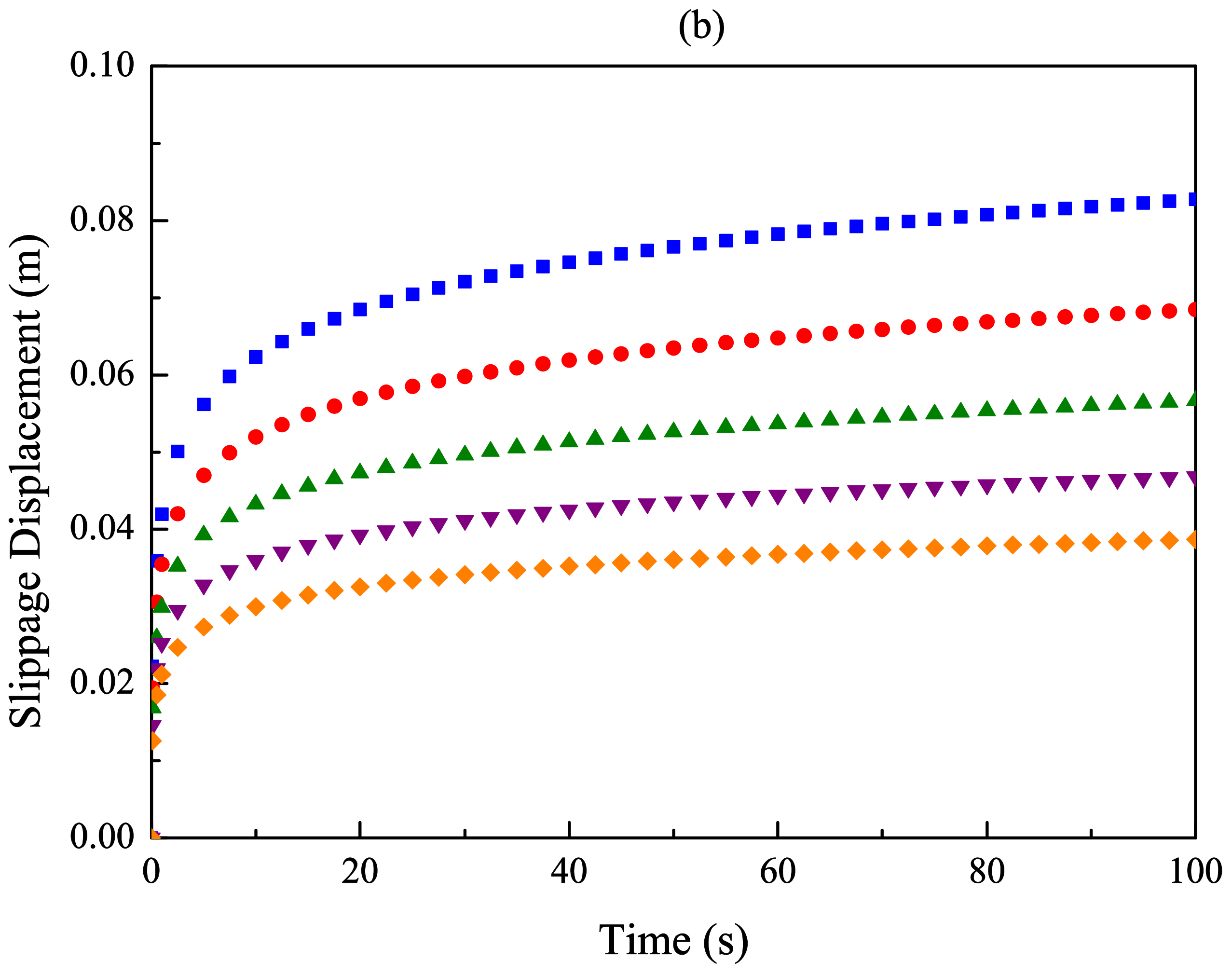
(b)
0.10
0.08
0.06
0.04
0.02
0.00
Slippage Displacement (m)
0
20
40
60
80
100
Time (s)

Figure 6 (a)

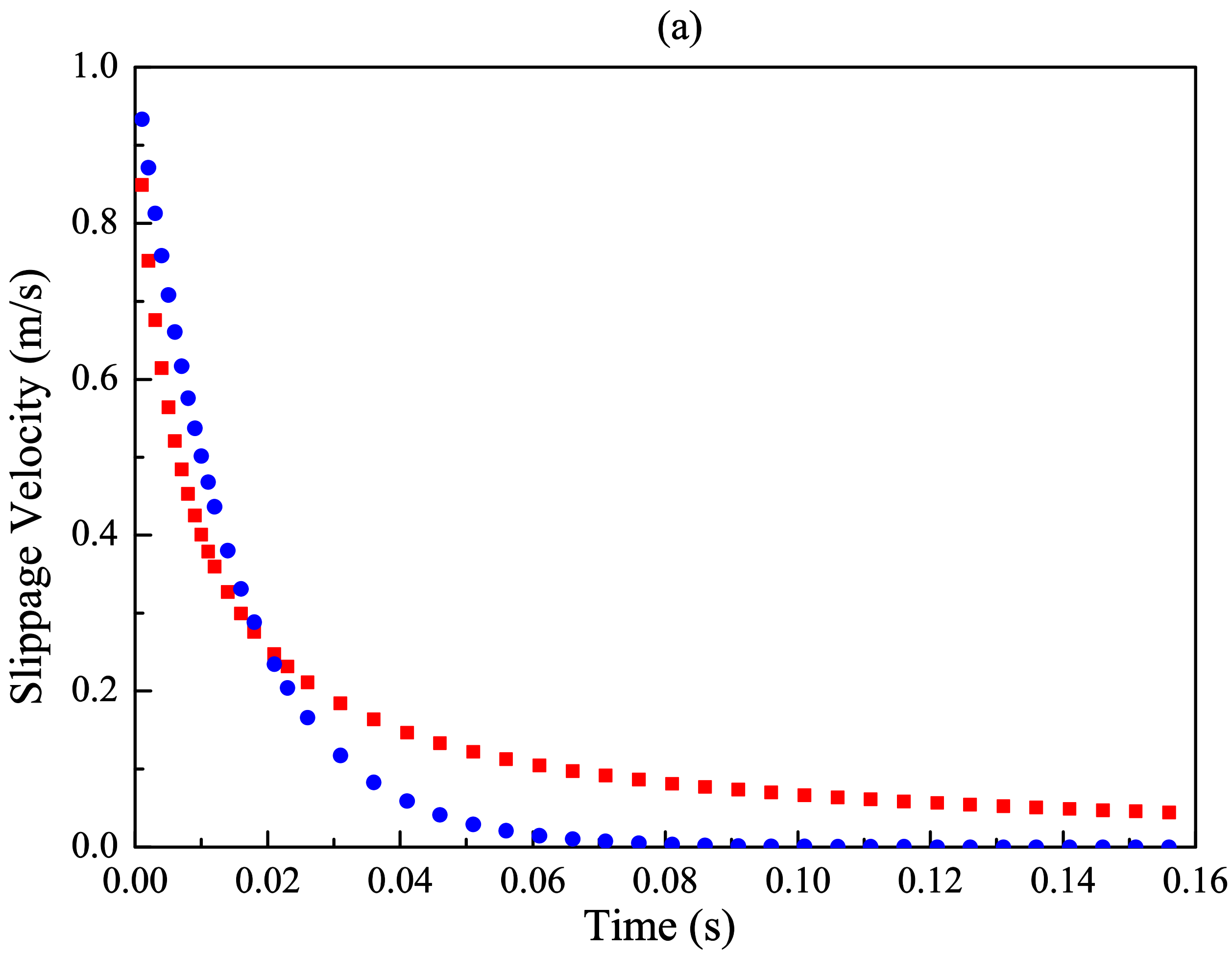

(a)
Slippage Velocity (m/s)
Time (s)
1.0
0.8
0.6
0.4
0.2
0.0
0.00
0.02
0.04
0.06
0.08
0.10
0.12
0.14
0.16

Figure 6 (b)

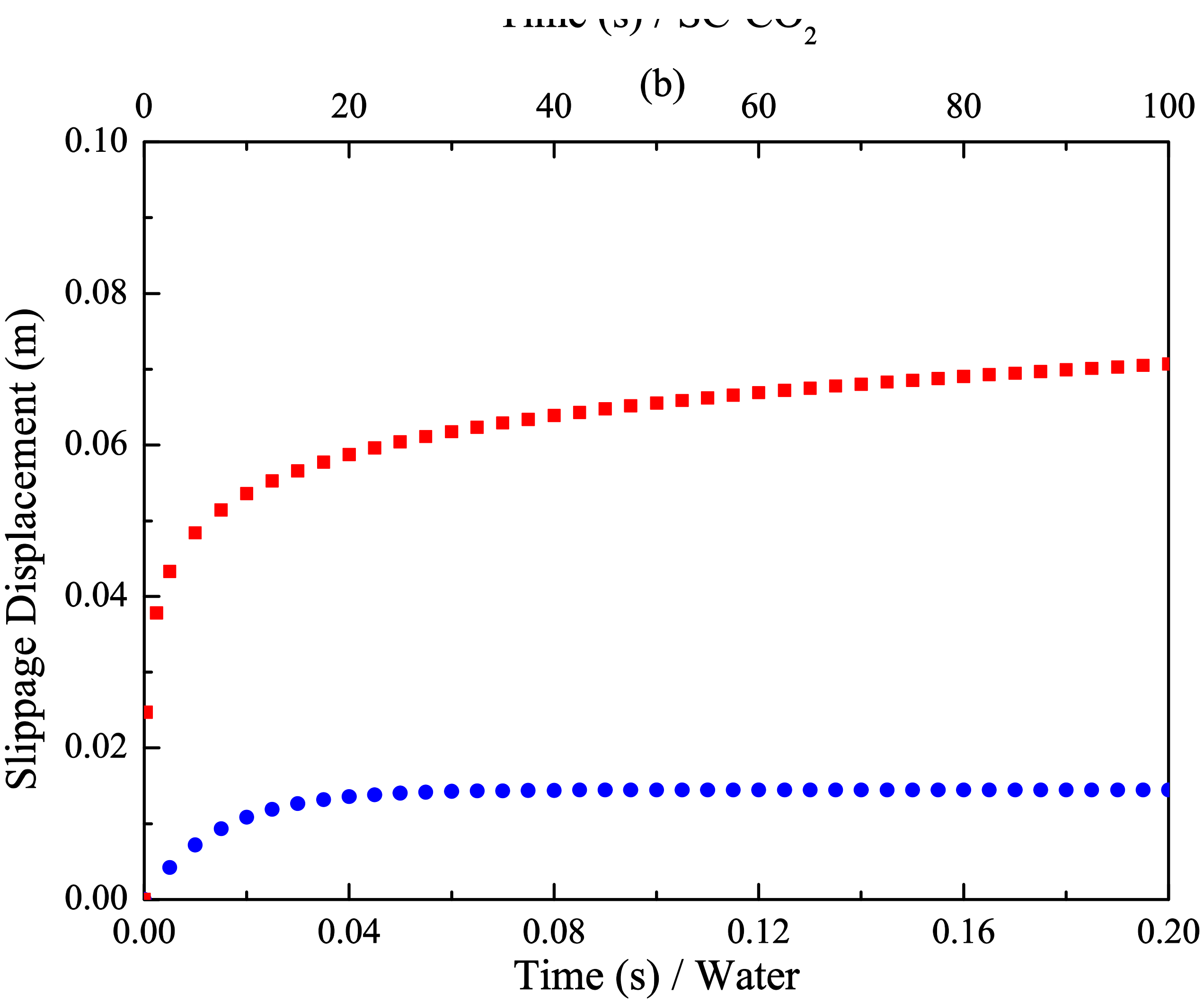

Time (s) / SC CO_2
(b)
0
20
40
60
80
100
0.10
0.08
0.06
0.04
0.02
0.00
Slippage Displacement (m)
0.00
0.04
0.08
0.12
0.16
0.20
Time (s) / Water

Table 1

Table 1

Experimental measured particle average velocity and slippage displacement

No.	Proppant condition		SC-CO_2 condition			Average particle velocity m/s	Average slippage displacement m
	ρ_p / kg/m³	d_p / mm	T / °C	P / MPa	v_f / m/s		
1	3120	0.3-0.6	45.9	10.96	1.085	0.991	0.0208
2	3120	0.3-0.6	47.5	10.91	0.920	0.827	0.0175
3	3120	0.3-0.6	46.7	9.52	1.284	1.204	0.0294
4	3120	0.3-0.6	40.8	7.89	1.087	0.924	0.0341
5	2630	0.425-0.85	43.0	8.89	0.958	0.843	0.0197
6	2630	0.425-0.85	44.8	8.27	1.170	1.026	0.0135
7	2630	0.425-0.85	46.2	9.58	1.025	0.964	0.0250
8	2630	0.425-0.85	38.6	7.89	1.128	0.992	0.0303

Table 2

Table 2

Velocity and displacement comparisons between measured and numerical results..

No.	Proppant condition		$SC\text{-}CO_2$ condition			Average velocity error %	Average displacement error %
	ρ_p / kg/m³	d_p / mm	T / °C	P / MPa	v_f / m/s		
1	3120	0.3-0.6	45.9	10.96	1.085	8.23	1.69
2	3120	0.3-0.6	47.5	10.91	0.920	4.05	3.57
3	3120	0.3-0.6	46.7	9.52	1.284	7.40	4.80
4	3120	0.3-0.6	40.8	7.89	1.087	5.30	5.49
5	2630	0.425-0.85	43.0	8.89	0.958	4.15	4.41
6	2630	0.425-0.85	44.8	8.27	1.170	7.95	1.25
7	2630	0.425-0.85	46.2	9.58	1.025	6.35	2.96
8	2630	0.425-0.85	38.6	7.89	1.128	3.48	2.05

Supplementary Material

Click here to download Supplementary Material: Supplementary---Experimental conditions in video.docx

Supplementary Material
Click here to download Supplementary Material: Figure 2.opj

Supplementary Material
Click here to download Supplementary Material: Figure 3.opj

Supplementary Material
Click here to download Supplementary Material: Figure 4.opj

Supplementary Material

Click here to download Supplementary Material: Supplementary---Lab Video.mp4

Supplementary Material
Click here to download Supplementary Material: Editorial Certificate.pdf